J Supercond Nov Magn (2014) 27:955–963
DOI 10.1007/s10948-013-2418-7

ORIGINAL PAPER

Cluster Size and Shape Effect on the Electronic Structure of the Hubbard Model Within the Norm-Conserving Cluster Perturbation Theory

Aleksandr Krinitsyn · Sergey Nikolaev · Sergey Ovchinnikov

Received: 19 September 2013 / Accepted: 28 September 2013 / Published online: 10 November 2013

Abstract Within a new norm-conserving approach to the cluster perturbation theory (CPT) for the 2d Hubbard model we study the effect of the cluster size and shape on the electronic structure. We have compared two type of clusters, 4-cluster (2×2) and 5-cluster (cruciform of 5 atoms). With 4-cluster we can treat exactly the first and second neighbours correlations, C_1 and C_2. With 5-cluster the third neighbour correlations C_3 are also treated exactly. The band structure in the CPT with 4- and 5-clusters differs remarkably. The quasiparticle spectral weight map for 5-clusters is very similar to the Quantum Monte Carlo (QMC) and the variational CPT data. With increasing doping, small hole Fermi surface transforms into conventional Fermi-liquid type large Fermi surface through Lifshitz quantum phase transitions.

Keywords Cluster perturbation theory · Hubbard model · Strong correlations · Density of states · Fermi surface

1 Introduction

Strong electron correlations (SEC) are known to determine many unusual properties of Mott-insulators like cuprates, manganites, cobaltites and other compounds characterized by interplay of spin, charge, and orbital degrees of freedom [1]. A theory of SEC systems is an actively developing field with different approaches being suggested (for example, [2–19]). Cluster perturbation theory (CPT) is a simple approximation scheme that applies to the Hubbard model as well as some other lattice models with local interaction. It can be viewed as a cluster extension of the perturbation theory from atomic limit [20] with the main advantage to incorporate nearest neighbour correlations at zeroth order of perturbation. Its features are found in more sophisticated approaches like the variational cluster approximation (VCA) [2] and the cellular dynamical mean field theory (C-DMFT) [3].

CPT has been proposed by several groups independently [6–10]; some reviews are available [11, 12]. The procedure of CPT consists of two steps: exact diagonalization (ED) of the independent individual cluster (unit cell) Hamiltonian H_0 and perturbation theory with the intercluster hopping and interaction H_1. In this paper we address the general aspect of the CPT. It concerns the effect of the cluster size and shape on the electronic structure. We will use a new version of theory, the norm-conserving CPT [13]. Usually, the Lanczos procedure is used for ED of H_0. It is fast because it does not consider all multielectron states of the cluster, only the ground state and a few excited. Our analysis [13] has shown that neglecting by a large part of excited states results in the lost quasiparticle (QP) spectral weight and strongly effects on the QP dispersion and spectral function $A(k, \omega)$. To control the conservation of the spectral weight we have introduced the f-factor (see definition below) that must be equal to 1 when all multielectron cluster states are taken into account.

For example, for the Hubbard model in the 2d square lattice the 2×2 cluster has 256 multielectron states $|N, i\rangle$

A. Krinitsyn
Dostoyevsky Omsk State University, Omsk 644077, Russia
e-mail: krinitss@mail.ru

S. Nikolaev · S. Ovchinnikov
Siberian Federal University, Krasnoyarsk 660041, Russia

S. Nikolaev
e-mail: 25sergeyn@mail.ru

S. Ovchinnikov (✉)
Kirensky Institute of Physics, Siberian Branch,
Russian Academy of Sciences, Krasnoyarsk 660036, Russia
e-mail: sgo@iph.krasn.ru

with different number of electrons $0 \leq N \leq 8$, and index i numerates the ground $|N,0\rangle$ and all excited terms with $i \neq 0$. For the half-filled band electron concentration per atom $n_e = 1$ the minimal set of states is given by $\{|3,0\rangle, |4,0\rangle, |5,0\rangle\}$. The number of cluster states is 5 ($|3,0\rangle$ and $|5,0\rangle$ has spin 1/2). For this minimal set we have found $f = 0.395$ [13]. It appears that specially selected finite set of cluster states (about 30 states) results in $f = 0.9995$. This is the main idea of norm-conserving CPT and the mathematical tool to handle the arbitrary large number of cluster multielectron states is given by the Hubbard operators $X^{N_1 i_1; N_2 i_2} = |N_1, i_1\rangle\langle N_2, i_2|$ [14, 20]. Here we want to compare QP electronic structure for two different clusters 2×2 square with 4 sites (4-cluster) and 5 sites cruciform one (5-cluster). Previously, the effect of cluster size and shape has been discussed in several papers [11, 15–17]. No essential difference was found for clusters of different shapes [15]. As concerns the size effect it is obvious that the more the better. In this paper we show that the QP dispersion and spectral weight distribution for 5-cluster is better than for 4-cluster (close to the Quantum Monte Carlo (QMC) [18], and variational CPT [19] data), that for the size effect. The shape effect is that the ground state energy E_0 is smaller for 4-cluster as against 5-cluster.

The paper is organized as follows: The norm-conserving cluster perturbation theory in X-representation is described in Sect. 2. It is shown how to find the Green's function for an infinite lattice and a scheme for the formation of Hubbard quasiparticles at nonzero doping value is presented. In Sect. 3 we study the electronic structure for the two forms of the basic clusters within NC-CPT. The dependence of the ground-state energy of the Coulomb interaction parameter U is calculated and results are compared with other theoretical works. The evolution of the Fermi surface of the hole concentration is presented in Sect. 4. The discussion of the results is provided in Sect. 5.

2 NC-CPT Method

In this section we briefly remind the norm-conserving cluster perturbation theory (NC-CPT) [13]. The Hubbard model is a good approximation to describe the two-dimensional square lattice with strong electron correlations [21]. This is one of the basic models for description of a large class of materials with the SEC. The Hamiltonian of the two-dimensional one-band Hubbard model is given by

$$H = \sum_{i\sigma}\left\{(\varepsilon-\mu)n_{i,\sigma} + \frac{U}{2}n_{i,\sigma}n_{i,\bar{\sigma}}\right\} - \sum_{i\neq j,\sigma} t_{ij}a^{\dagger}_{i\sigma}a_{j\sigma}, \quad (1)$$

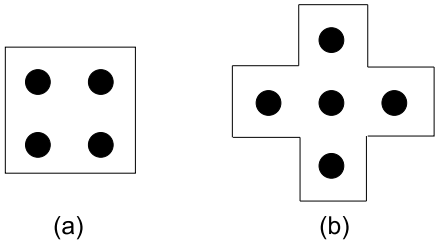

Fig. 1 (**a**) The cluster 2×2 with $N_{\text{sites}} = 4$; (**b**) the cruciform cluster with $N_{\text{sites}} = 5$

where ε is an energy of electron at a site, μ is chemical potential, U is the parameter of the Coulomb repulsion, $a^{\dagger}_{i\sigma}$ and $a_{i\sigma}$ are the creation and annihilation operators of an electron on the site i with spin σ ($\bar{\sigma} = -\sigma$), $n_{i\sigma} = a^{\dagger}_{i\sigma}a_{i\sigma}$ is the particle number operator, t_{ij} is the hopping integral from site j to site i.

Let us choose a cluster of such a form that it can be the unit cell for the original square lattice. In this paper, we have used the 5-cluster and 4-cluster (Fig. 1). We can separate the Hamiltonian (1) in two parts with intra- and inter-cluster interaction terms

$$H = \sum_{f} H_0(f) + \sum_{f\neq g} H_t(f,g), \quad (2)$$

where f, g are cluster indexes. Next step of calculation includes computing a complete set of eigenstates and eigenvectors of the Hamiltonian $H^c_0(f)$ by exact diagonalization method. These eigenstates allow us to construct the cluster X-operators and to write Hamiltonian H in X-representation. So we can write the annihilation operator of an electron at a site i for cluster f in the following exact representation:

$$a_{fi\sigma} = \sum_{\alpha}\gamma_{i\sigma}(\alpha)X^{\alpha}_{f}, \qquad \gamma_{i\sigma}(\alpha) = \langle n|a_{fi\sigma}|m\rangle. \quad (3)$$

Here we use the following notation for the X-operators: $X^{\alpha}_{f} = X^{nm}_{f} = |n\rangle\langle m|$, where $\alpha = \alpha(n,m)$, m and n are initial and final states of the cluster, respectively, and f is the cluster index. The properties of X-operators are described in [14, 20, 22]. This expression allows to consider electron as superposition of different quasiparticles (Hubbard fermions) X^{α}_{f}. Moreover, each quasiparticle corresponds to the excitation with charge e and spin $s = 1/2$ from the initial many-particle state $|m\rangle$ to final many-particle state $|n\rangle$. This procedure is described in [13] with more details.

The transformed Hamiltonian (2) is given by

$$H = \sum_{fn}\varepsilon_n X^{nn}_{f} + \sum_{f\neq g}\sum_{\alpha\beta} t^{\alpha\beta}_{fg}X^{\dagger\alpha}_{f}X^{\beta}_{g}, \quad (4)$$

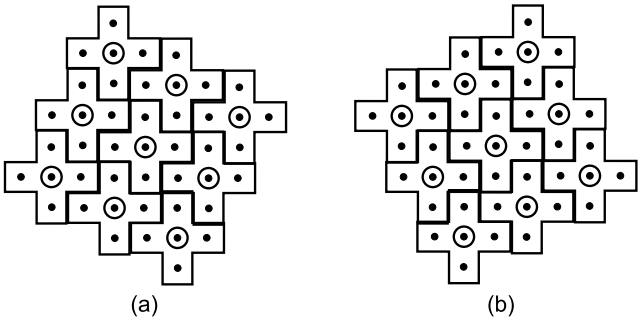

Fig. 2 The possible covering of the initial square lattice by cruciform clusters with five sites. The *dots* indicate the sites of the original lattice, *mugs* indicate sites of the cluster superlattice. In the text the notation of coverings $K1$ (**a**), $K2$ (**b**) is used

where ε_n is an energy of the cluster in the state n, and $t_{fg}^{\alpha\beta}$ are the intercluster hopping integrals.

After Fourier transformation the inter-cluster interaction part of the Hamiltonian (4) has the form

$$H_t = \sum_{\tilde{\mathbf{k}}} \sum_{\alpha\beta} T_{\alpha\beta}(\tilde{\mathbf{k}}) X_{\tilde{\mathbf{k}}}^{\dagger\alpha} X_{\tilde{\mathbf{k}}}^{\beta}, \tag{5}$$

where $\tilde{\mathbf{k}}$ is a wavevector in the reduced Brillouin zone.

As is with most versions of CPT, we have used the "Hubbard-I" approximation for the inter-cluster hopping $T_{\alpha\beta}(\tilde{\mathbf{k}})$ and obtained a solution for the Green function $D_{\alpha\beta}(\tilde{\mathbf{k}}, \omega) = \langle\langle X_{\tilde{\mathbf{k}}}^{\alpha} | X_{\tilde{\mathbf{k}}}^{\dagger\beta} \rangle\rangle_{\omega}$ in the following matrix form:

$$D^{-1}(\tilde{\mathbf{k}}, \omega) = \big(D^0(\omega)\big)^{-1} - T(\tilde{\mathbf{k}}), \tag{6}$$

where

$$D_{\alpha\beta}^0(\omega) = \frac{F(\alpha)}{\omega - \Omega(\alpha)} \delta_{\alpha\beta}, \tag{7}$$

$$\Omega(\alpha) = \varepsilon_m(N+1) - \varepsilon_n(N) - \mu, \tag{8}$$

$$F(\alpha) = F(n,m) = \big\langle X^{nn} \big\rangle + \big\langle X^{mm} \big\rangle. \tag{9}$$

Here $D^0(\omega)$ is the local (cluster) Green function, $F(\alpha)$ is the filling factor, μ is the chemical potential, and N is the number of electrons in the cluster.

The Green function $G_{\sigma}(\mathbf{k}, \omega) = \langle\langle a_{\mathbf{k}\sigma} | a_{\mathbf{k}\sigma}^{\dagger} \rangle\rangle_{\omega}$ that is defined on the original lattice is associated with the Green function in X-representation that is defined on the superlattice in the following way [13, 15]:

$$G_{\sigma}(\mathbf{k}, \omega) = \frac{1}{N_c} \sum_{\alpha\beta} \sum_{i,j=1}^{N_c} \gamma_{i\sigma}(\alpha) \gamma_{j\sigma}^*(\beta) \times D_{\alpha\beta}(\mathbf{k}, \omega) e^{-i\mathbf{k}(\mathbf{r}_i - \mathbf{r}_j)}, \tag{10}$$

where N_c is the number of sites in the cluster (in this case, 4 and 5), $\mathbf{k}$ is the wavevector defined in the original Brillouin zone, i and j are intra-cluster sites indices. By the definition, the spectral function

$$A_{\sigma}(\mathbf{k}, \omega) = -\frac{1}{\pi} \lim_{\delta \to 0^+} \big(\operatorname{Im} G_{\sigma}(\mathbf{k}, \omega + i\delta + \mu)\big). \tag{11}$$

We control the value of f-factor in all calculations carried out in this paper. This parameter introduced in [13] is a measure of the total spectral weight of Fermi quasiparticles,

$$\int d\omega A_{\sigma}(\mathbf{k}, \omega) = \sum_{\alpha} \big|\gamma_{i\sigma}(\alpha)\big|^2 F(\alpha) \equiv f; \tag{12}$$

$f = 1$ for an exact calculation. But in this case it is necessary to take into account the complete set of eigenstates of the cluster, which makes the problem intractable. It was found that it is possible to take into account smaller set of cluster eigenstates with the value of f-factor close to 1, and the error in the final result will not exceed a few per cent. Moreover, we can significantly reduce the computation time without distorting the results by controlling this value. All the following results were obtained with $f > 0.95$.

The cruciform cluster gives us two independent ways to cover the original square lattice (see Fig. 2). The procedure of covering was described in [23] for a square cluster 2×2. Arguments in [23] allow to construct a linear superposition of solutions of two coverings ($K1$ and $K2$) by an averaging of a hopping matrix, which determines the inverse Green function (6),

$$T_{\alpha\beta}(\mathbf{k}) = \frac{1}{2}\big(T_{\alpha\beta}^{K1}(\mathbf{k}) + T_{\alpha\beta}^{K2}(\mathbf{k})\big), \tag{13}$$

where $\mathbf{k}$ is the wavevector in the original Brillouin zone. As shown in [23], this procedure determines the Green function (6) in the original Brillouin zone, and the Green function (10) has the symmetry of a square lattice.

In this paper we carry out the study of the electronic structure of systems with SEC for various doping p (hole density per site). For instance, in Fig. 3 the low-energy part of the Hilbert space of a single cluster with five sites is schematically shown. At half-filling (undoped) and $T = 0$ the excitations between the ground state in the subspace with

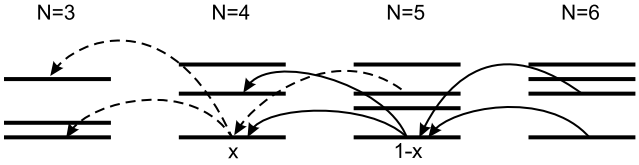

Fig. 3 The scheme of the low energy part of the Hilbert space for the 5-site cluster. For hole concentration $p = x/5$ the ground-state term with $N = 5$ is filled with probability $1 - x$, and the term with $N = 4$ with probability x. All other states are empty at $T = 0$. *Solid arrows* denote electron annihilation process in the case without doping ($x = 0$), the *dashed arrows* denote additional excitations that must be considered in doped case ($x \neq 0$). N is the number of electrons in the cluster

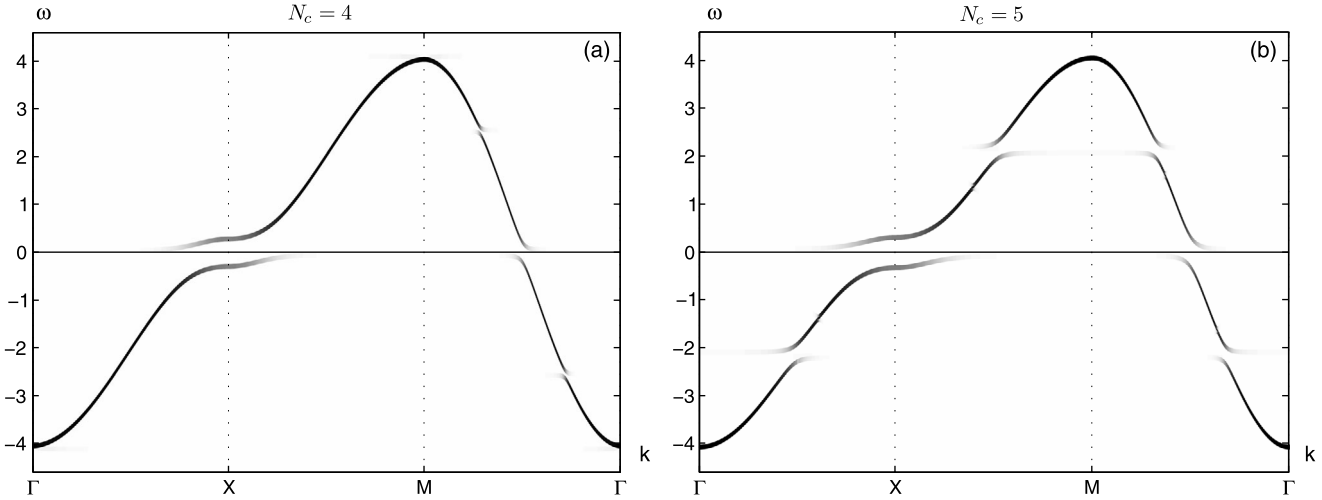

Fig. 4 Dispersion curves for the undoped case and $U = 1$ along the symmetry directions $\Gamma \to X \to M \to \Gamma$ in the first quadrant of the first Brillouin zone ((**a**) for the cluster 2×2, (**b**) for the cruciform cluster). Here and below we use the notation: $\Gamma = (0, 0)$, $X = (\pi, 0)$, $M = (\pi, \pi)$. The line intensity is proportional to the QP spectral weight

$N = 5$ and states in the subspaces with $N = 4$ and $N = 6$ have nonzero filling factor (9) (in Fig. 3 this transitions are marked by solid arrows). It is necessary to consider the possibility of population of the ground state in the subspace with $N = 4$ for hole doping. This results in the additional excitations with nonzero filling factor (marked by dashed arrows in Fig. 3). It should be noted that we consider only the one-electron excitations with change in the number of particles ± 1. In the case of 5-cluster the cluster doping x and doping on the site p are related by $x = 5p$.

3 Band Structure and Ground State Energy

We plot the QP dispersion curves for the 4-cluster and the 5-cluster in Fig. 4 ($U = 1$) and Fig. 5 ($U = 8$) for undoped model with $n_e = 1$. The energy scale is given by $t = 1$, where t is the nearest neighbour hopping parameter. As was shown long ago by Hubbard, in the paramagnetic state the free electron band is split and the lower (LHB) and upper (UHB) Hubbard bands are separated by the Mott–Hubbard gap. It is clearly seen in Fig. 4(a) for 4-cluster. For 5-cluster (Fig. 4(b)) we can see the additional splitting of the UHB and LHB. Similar splitting has been obtained due to the long-range antiferromagnetic (AFM) superstructure [24]. In this paper we have consider only paramagnetic phase with a shot-range antiferromagnetic correlations. In the 4-cluster the ED incorporate the first neighbours correlation function C_1 and the second neighbour function C_2, while in the 5-cluster the third neighbour correlation function C_3 is additionally present. Thus the difference in Fig. 4(a, b) is a typical size effect. Similar splitting of the LHB and UHB in the paramagnetic phase has been obtained by QMC [18] and V-CPT [19] methods. Comparison of QMC and V-CPT data and our calculations for $U = 8$ is shown in Fig. 5. The different distribution of the QMC spectral weight is the other size effect. The difference is clearly observed for the LHB in the Γ point and for the UHB in the M point. In general, both the dispersion curves and the intensity map of Fig. 5(b) (5-cluster) are similar to the QMC and V-CPT data, but not in Fig. 5(a) for 4-cluster. Thus, the adding of the third correlation C_3 strongly affects the dispersion and the intensity map.

The splitting of the Hubbard bands can be seen also in the density of states. In Fig. 6 the density of states within NC-CPT approach for the 4-cluster, the 5-cluster and the C-DMFT [25] is shown for half-filled band and $U = 8$ for the model with nearest neighbours hopping. A comparison of Fig. 6(b, c) shows a qualitative agreement of the results, in particular the presence of a gap in the range of $4t > |\omega| > 3t$. However, Fig. 6(a) shows that such gap for the 4-cluster is not observed. Figure 6 also shows that the C-DMFT gives a lower value of the Mott–Hubbard gap than the NC-CPT gap. While the Mott–Hubbard gap Δ results from charge fluctuations, the additional gap Δ' appears in the long-range AFM or quite extended short-range AFM state. It may be called a magnetic gap. In Fig. 7 the dependence of the magnetic gap Δ' as a function U is shown. It is seen that this gap saturates with increasing the Coulomb parameter U.

We calculated the energy of the ground state of an infinite lattice taking into account hopping only between nearest neighbours. In our case, we use the expression from [15, 26] to calculate the ground state energy per site:

$$E_0 = \frac{1}{2N} \sum_{\sigma \mathbf{k}} \int_{-\infty}^{0} d\omega (\varepsilon_{\mathbf{k}} + \omega + \mu) A_\sigma(\mathbf{k}, \omega). \tag{14}$$

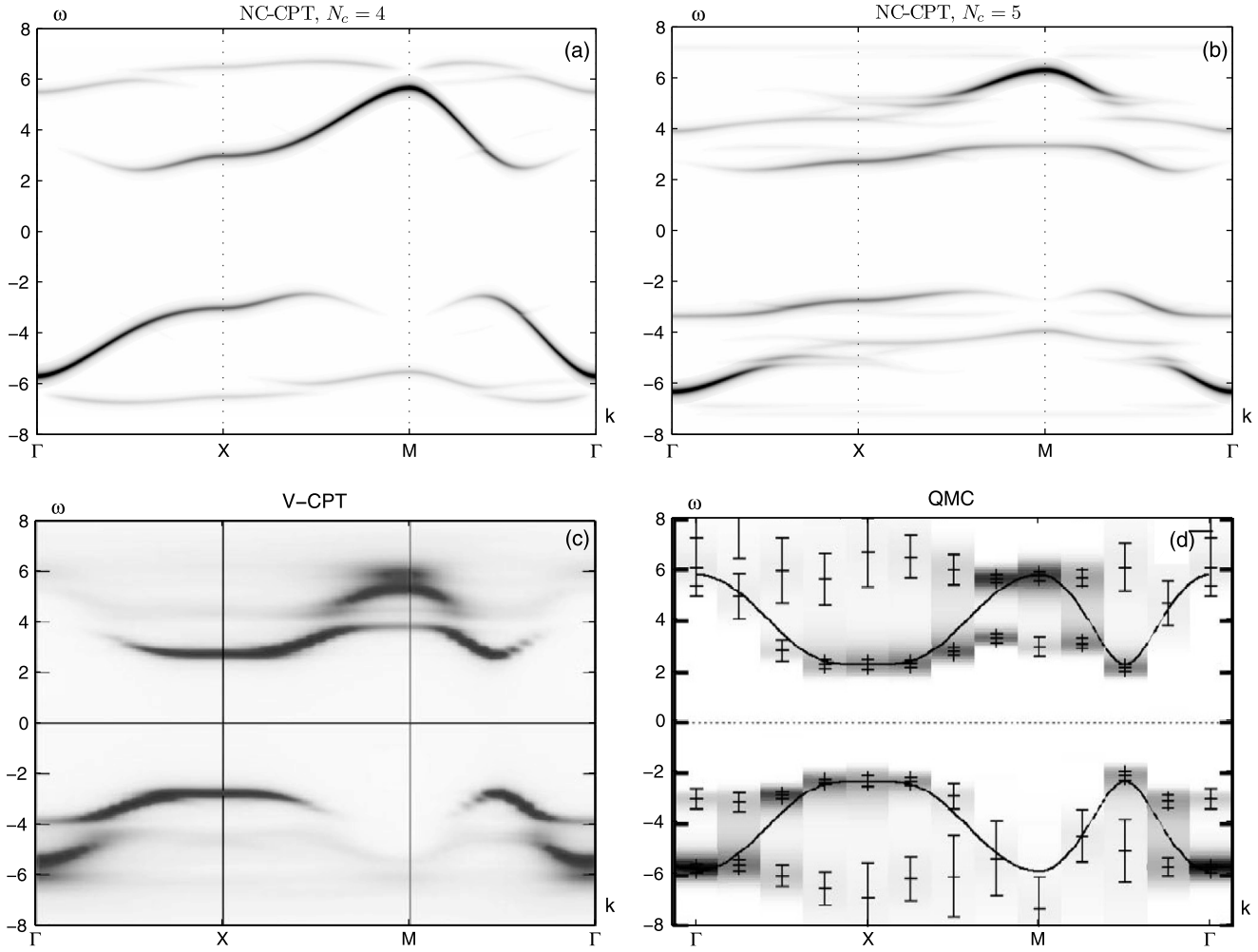

Fig. 5 Dispersion curves for the undoped case for $U = 8$ along the symmetry directions $\Gamma \to X \to M \to \Gamma$ in the first quadrant of the first Brillouin zone ((**a**) for the cluster 2×2, (**b**) for the cruciform cluster, (**c**) V-CPT [19], (**d**) QMC [18])

Here, $\varepsilon_{\mathbf{k}} = -2t(\cos(k_x) + \cos(k_y))$ is the free electron spectrum (lattice constant is taken as unity), $\mathbf{k}$ is wave vector in the original Brillouin zone, N is number of sites in the initial lattice.

In Fig. 8 the dependence of the ground state energy per site E_0 calculated by different methods (including nonperturbative) as function of U is shown. We see that our calculation for the cruciform cluster gives the value E_0 higher than in other works [19, 27–29], but for the cluster 2×2 our E_0 is in good agreement with the other works.

We consider this difference to be a shape effect. In the 2×2 cluster all sites are equivalent, while in the cruciform 5-cluster the central site is similar to a "bulk atom" and all the others are the "surface atoms" with three dangling bonds. Indeed, in a 2×2 square cluster we take into account four first correlations C_1 and two second correlations C_2; per site it gives $1C_1 + 0.5C_2$. In the cruciform 5-cluster we take into account $4C_1 + 4C_2 + 2C_3$; per site it gives $0.8C_1 + 0.8C_2 + 0.4C_3$. It is clear that the shortest bonds are stronger, so smaller is the nearest neighbour contribution in the case of 5-cluster results in the higher energy E_0.

4 The Doping Transformation of the Fermi Surface

There are two aspects of the transformation of the Fermi surface (FS) with the hole concentration in the study of high-T_c cuprates. This is (i) a change in the topology of the Fermi surface [30] and (ii) non-uniform redistribution of the quasiparticle spectral weight along the FS (Fermi arc [31–33]). Usually this behaviour is related to the presence of short-range AFM order. The cluster approach is able to directly account for this order and to assess its effect on the spectrum of quasiparticles. We will calculate the Fermi surface for different doping concentrations by two ways, from the poles of the electronic Green function at $\omega = \epsilon_F$ and from the spectral density map $A(\mathbf{k}, \epsilon_F)$ that is related to ARPES

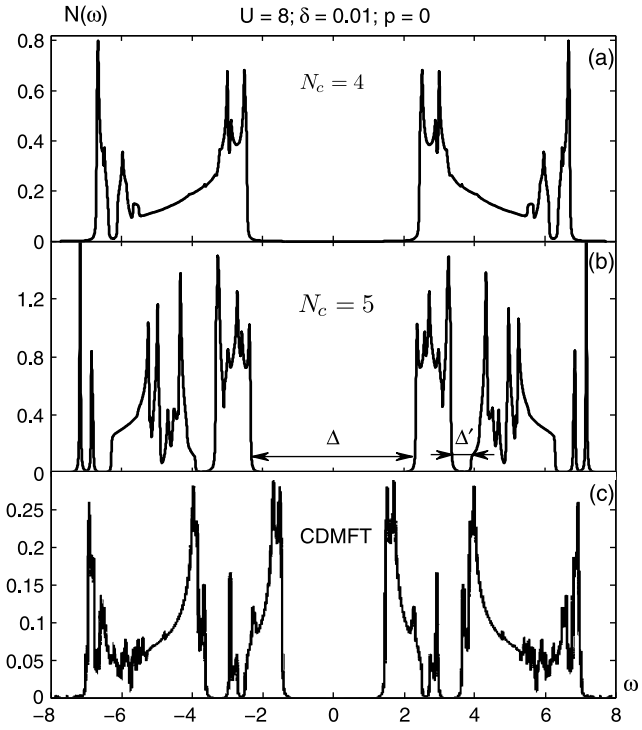

Fig. 6 The density of states for the undoped case at $U = 8$ ((**a**) for the 4-cluster, (**b**) for the 5-cluster, (**c**) CDMFT [25]). The parameter of the Lorenz linewidth for the spectra line, $\delta = 0.01$. Δ is the Mott–Hubbard gap, Δ' is the gap in the Hubbard sub-bands

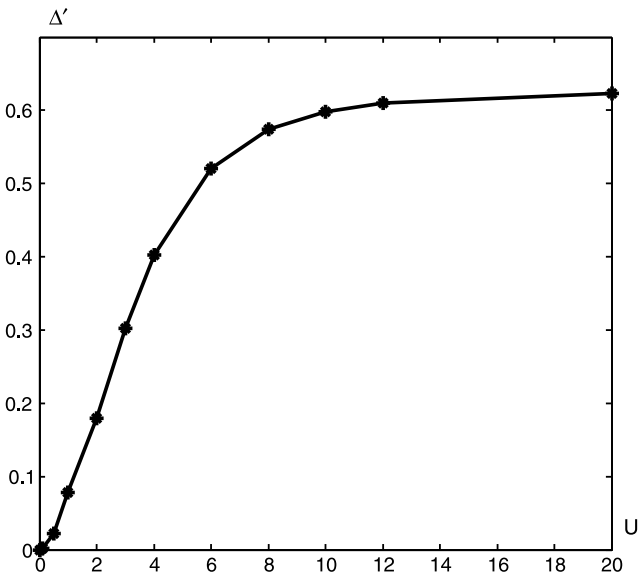

Fig. 7 The magnetic gap Δ' as a function of U

data [34, 35]. In the numeric computation of spectral density we substitute a delta-function by a Lorenzian curve with a broadening parameter $\delta \ll t$. It allows to model experimental resolution of ARPES and finite QP lifetime that may appear due to high order perturbation contributions from the intercluster hopping.

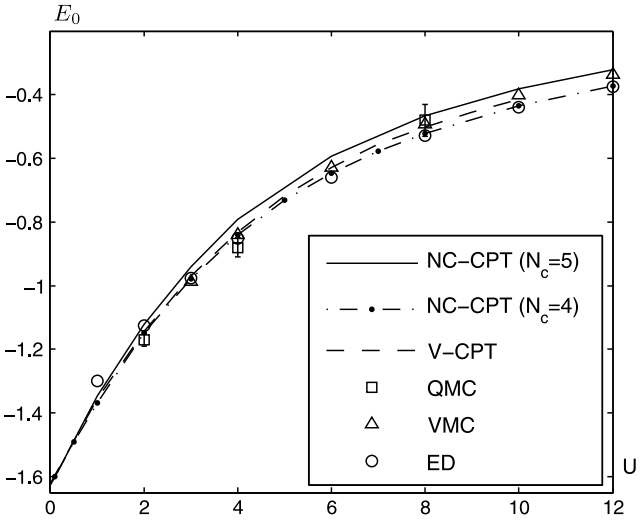

Fig. 8 The ground-state energy E_0 in undoped case vs the parameter U. *Solid curve* is for our calculation for the cruciform cluster; *dashed curve* is for variational cluster perturbation theory (V-CPT) [19]; *triangles* are for Variational Monte Carlo (VMC) [27]; *circles* are the exact diagonalization (ED) of the cluster 4×4 [29]; *squares* are Quantum Monte Carlo (QMC) [28]; *dot-dashed curve with dots* is NC-CPT for a cluster 2×2 [23]

The doping-dependent QP density of states (DOS) for the LHB and position of the Fermi level are shown in Fig. 9. For $p = 0.01$, the in-gap states appears above the top of the LHB. For $p > 0.05$, the in-gap band is connected with the LHB. The Fermi level lies in the region of depleted DOS for $0.01 < p < 0.12$ that may be related to the pseudogap state.

The $A(k_x, k_y, \epsilon_F)$ maps are shown in Fig. 10. For small concentration, $p = 0.01$, the Fermi surface consists of 4 small hole pockets (Fig. 10(a)) with a centre along the line $(\pi/2, \pi/2) - (\pi, \pi)$. Different parts of the pocket have different spectral weight, the largest one in the nodal direction at the side directed to the Γ point and the minimal at the side directed to the (π, π) point. The small hole pocket near $(\pi/2, \pi/2)$ has been found in a doped Mott insulator due to the long or shot range AFM order by ED [36, 37] and [38, 39] for the finite clusters as well as by a perturbation treatment of the infinite lattice [40–43] and using slave-particles [44, 45]. The spectral weight distribution along the Fermi pocket has been obtained previously by several groups [46–48] due to the hole scattering on spin fluctuations. This is one of the evidences of the pseudogap state.

With doping increase the Fermi surface changes its topology as can be seen in Fig. 10. Similar changes have been obtained within the t-J-model [30] and have been discussed as the Lifshitz quantum phase transitions (QPT) [49, 50]. The first QPT is related with the change of connectivity, four closed small pockets transform at $p = p_{c1}$ into two large surface centred at (π, π). The large one has the large spectral weight while the smaller surface has the small spectral weight (Fig. 10(b)). There is also a line of zeros of the

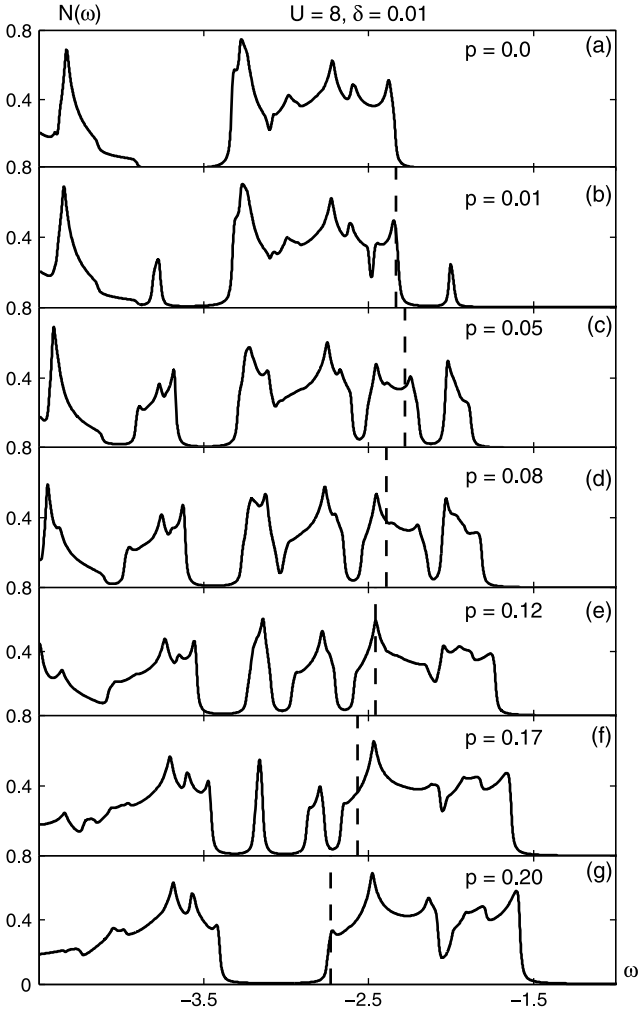

Fig. 9 The density of states for doping $p = 0.0, 0.01, 0.05, 0.07, 0.12, 0.17, 0.20$. The *vertical dotted line* marks the position of the Fermi level. The model parameters are $U = 8$, $t' = t'' = 0$; the broadening $\delta = 0.01$

spectral function around (π, π), previously obtained by the CDMF method [25, 51]. With further doping increase the smaller surface meets the line of zeros at $p = p_{c2}$, and they annihilate each other. At this second QPT the number of Fermi surfaces changes. Above the p_{c2} there is one large hole Fermi surface (Fig. 10(c)) that corresponds to the Fermi liquid behaviour with the volume $\sim n_h = 1 + p$. Finally, with further doping increase there is the third Lifshitz transition from the hole surface around (π, π) to the electronic surface around Γ point, it occurs at $p_{c3} = 0.12$ (Fig. 10(d)). Previously a similar transition has been discussed in Ref. [52]. Further doping results in a similar transformation of the electronic Fermi-surface (Fig. 10(e, f)). The critical concentration strongly depends on parameters, so they are different than in Refs. [30, 49, 50]. Here we have studied the general properties of Hubbard model without fitting the cuprates electronic structure by second and third neighbour hoppings t' and t''. The Fermi surface topology and the type of its changes are the general property, which is the same here and in the more realistic model [30].

To compare the spectral function map to the ARPES data, we have plotted the $A(k_x, k_y, \epsilon_F)$ maps with larger value of the linewidth parameter $\delta = 0.05t$ (Fig. 11) and $\delta = 0.1t$. Instead of the closed small pocket we obtain the arc (Fig. 11(a)) that becomes larger in Fig. 11(b, c). This behaviour is typical to the ARPES conclusion on the doping evolution of the Fermi surface in cuprates. To measure the fine details and QPT by ARPES the better resolution should be used.

In previous CPT calculations the Fermi surface has been discussed for a few concentrations. Thus, for $p = 0.17$ the large Fermi surface has been obtained for $U = 2$, and the arc has been found for $U = 8$ [53]. The small hole pocket in the underdoped region has been obtained by variational CPT [54]. Similarly to our data the evolution of the Fermi surface has been found by the C-DMFT calculations [25], by perturbation theory from the atomic limit [55, 56], in a spin density wave fluctuation approach to the Hubbard model [57, 58], and the multielectron configuration quantum-chemistry calculation [59].

5 Conclusions

The comparison of 4-cluster and 5-cluster CPT has revealed that the exact treatment of first, second and third neighbour correlations in the 5-cluster results in the QP band structure and the spectral weight distribution that is in a good agreement to the Quantum Monte Carlo [18], V-CPT [19], and C-DMFT [25] methods, while the 4-cluster CPT calculations do not reproduce the LHB and UHB splitting by the short range order AFM fluctuations. This is the size effect in our CPT theory.

The shape effect was found in the ground state energy E_0. For all values of U, the 4-cluster E_0 is less than the 5-cluster E_0. We relate this with the dominant contribution of the most stronger nearest neighbour correlations.

We have studied the hole doping dependence of the QP band structure and the Fermi surface within 5-cluster CPT. We have reproduced the cascade of the quantum phase transitions of the Lifshitz type with increasing doping that has been obtained previously by the X-operators perturbation theory [30] with static shot-range AFM correlations. In the present approach both the static and dynamical correlations inside each cluster are treated exactly. That is why it allows to describe both the shape of the Fermi surface and the nonuniform spectral weight distribution along the Fermi contour. The increase of the broadening parameter transforms the small hole pocket in the underdoped region in the arc. Previously a similar conclusion has been found by C-DMFT method [25].

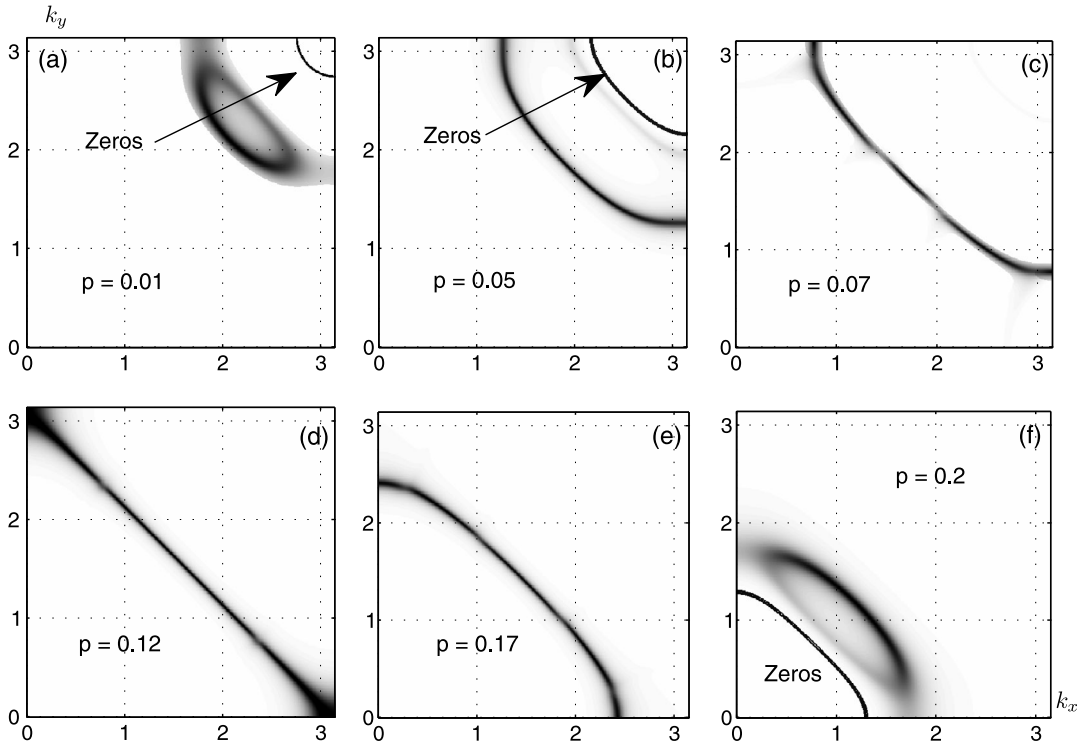

Fig. 10 The maps of the spectral weight for doping $p = 0.01, 0.05, 0.07, 0.12, 0.17, 0.20$. The model parameters are $U = 8$; the broadening $\delta = 0.01$

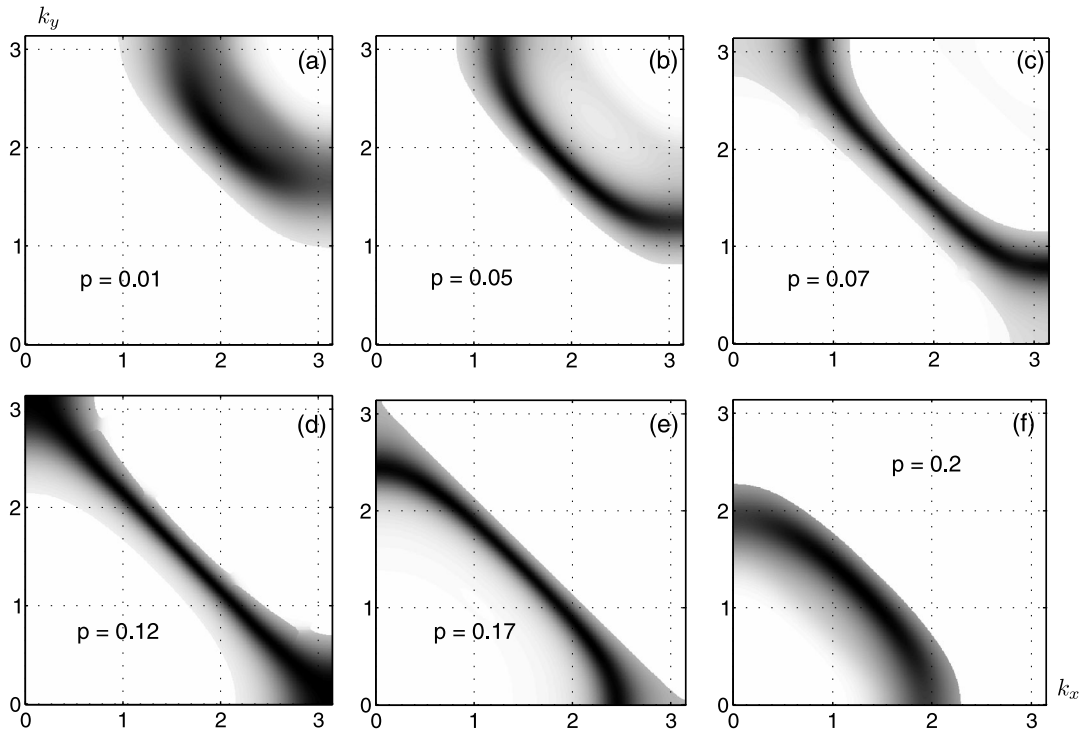

Fig. 11 The same as in Fig. 10 with the broadening $\delta = 0.05$

One important physical result obtained by our CPT approach concerns the problem of Fermi arcs versus closed Fermi contours in cuprates. While ARPES results in the weakly doping dependent Fermi arcs, the quantum oscillations measurements have revealed the closed pockets. Our calculations of the spectral weight map have found the strong dependence on the spectral line width that is related to the experimental resolution. At low resolution typical to ARPES 10–15 years ago our theory results in the Fermi arc with small doping dependence. For better resolution of the modern ARPES we predict the closed pockets seen in the dHvA experiments. Thus we suggest to ARPES community to repeat the Fermi surface study with the state-of-art resolution (for example, with energy resolution $\sim$2 meV).

Acknowledgement This work was supported by Grants NSh-1044.2012.2 and MK-1168.2012.2, Siberian Federal University: Grant F-11, and the Presidium of RAS Program 20.7.

References

1. Maekawa, S., Tohyama, T., Barnes, S.E., et al.: Physics of Transition Metal Oxides. Springer, Berlin (2004)
2. Potthoff, M., Aichhorn, M., Dahnken, C.: Phys. Rev. Lett. **91**, 206402 (2003)
3. Kotliar, G., Savrasov, S., Palsson, G., Birali, G.: Phys. Rev. Lett. **87**, 186401 (2001)
4. Knetter, C., Schmidt, K.P., Uhrig, G.S.: Eur. Phys. J. B **36**, 525 (2003)
5. Raas, C., Grete, P., Uhrig, G.S.: Phys. Rev. Lett. **102**, 076406 (2009)
6. Barabanov, A.F., Maksimov, L.A., Mikheenkov, A.V.: Sov. Phys., Solid State **30**, 1449 (1988)
7. Barabanov, A.F., Maksimov, L.A., Mikheyenkov, A.V.: J. Phys. Condens. Matter **1**, 10143 (1989)
8. Ovchinnikov, S.G., Sandalov, I.S.: Physica C **161**, 607 (1989)
9. Gros, C., Valenti, R.: Phys. Rev. B **48**, 418 (1993)
10. Senechal, D., Perez, D., Pioro-Ladriere, M.: Phys. Rev. Lett. **84**, 522 (2000)
11. Maier, T., Jarrell, M., Pruschke, T., Hettler, M.H.: Rev. Mod. Phys. **77**, 1027 (2005)
12. Senechal, D.: Strongly Correlated Systems. In: Avella, A., Mancini, F. (eds.): Theoretical Methods, Cluster Perturbation Theory, vol. 171. Springer, Berlin (2011)
13. Nikolaev, S.V., Ovchinnikov, S.G.: J. Exp. Theor. Phys. **111**, 635 (2010)
14. Ovchinnikov, S.G., Val'kov, V.V.: Hubbard Operators in the Theory of Strongly Correlated Electrons. Imperial College Press, London (2004)
15. Senechal, D., Perez, D., Plouffe, D.: Phys. Rev. B **66**, 075129 (2002)
16. Jarrell, M., Maier, Th., Huscroft, C., Moukouri, S.: Phys. Rev. B **64**, 195130 (2001)
17. Tremblay, A.-M.S., Kyung, B., Senechal, D.: Low Temp. Phys. **32**, 424 (2006)
18. Grober, C., Eder, R., Hanke, W.: Phys. Rev. B **62**, 4336 (2000)
19. Dahnken, C., Aichhorn, M., Hanke, W., et al.: Phys. Rev. B **70**, 245110 (2004)
20. Hubbard, J.: Proc. R. Soc. A **285**, 542 (1965)
21. Hubbard, J.: Proc. R. Soc. A **276**, 238 (1963)
22. Zaitsev, R.O.: Sov. Phys. JETP **41**, 100 (1975)
23. Nikolaev, S.V., Ovchinnikov, S.G.: J. Exp. Theor. Phys. **114**, 118 (2012)
24. Ovchinnikov, S.G., Shneider, E.I.: Phys. Solid State **46**, 1469 (2004)
25. Sakai, S., Motome, Y., Imada, M.: Phys. Rev. B **82**, 134505 (2010)
26. Kittel, C.: Quantum Theory of Solids. Wiley, New York (1963)
27. Yokoyama, H., Shiba, H.: J. Phys. Soc. Jpn. **56**, 3582 (1987)
28. Hirsch, J.E.: Phys. Rev. B **31**, 4403 (1985)
29. Fano, G., Ortolani, F., Parola, A.: Phys. Rev. B **42**, 6877 (1990)
30. Korshunov, M.M., Ovchinnikov, S.G.: Eur. Phys. J. B **57**, 271 (2007)
31. Yoshida, T., Zhou, X.J., Lu, D.H., et al.: J. Phys. Condens. Matter **19**, 125209 (2007)
32. Hashimoto, M., Yoshida, T., Yagi, H., et al.: Phys. Rev. B **77**, 094516 (2008)
33. Doiron-Leyrand, N., Proust, C., LeBoeuf, D., et al.: Nature **447**, 565 (2007)
34. Damascelli, A., Hussain, Z., Shen, Z.: Rev. Mod. Phys. **75**, 473 (2003)
35. Kanigel, A., Norman, M.R., Randeria, M., et al.: Nat. Phys. **2**, 447 (2006)
36. Horsch, P., Stephan, W., von Szczepanski, K.J., et al.: Physica C **162**, 783 (1989)
37. Dagotto, E.: Rev. Mod. Phys. **66**, 783 (1994)
38. Preuss, R., Hanke, W., van der Linden, W.: Phys. Rev. Lett. **75**, 1344 (1995)
39. Elesin, V.F., Kashurnikov, V.A.: J. Exp. Theor. Phys. **79**, 961 (1994)
40. Shraiman, B.I., Siggia, E.D.: Phys. Rev. Lett. **61**, 467 (1988)
41. Trugman, S.A.: Phys. Rev. Lett. **65**, 500 (1990)
42. Barabanov, A.F., Kuzian, R.O., Maksimov, L.A.: J. Phys. Condens. Matter **3**, 91129 (1991)
43. Chen, Q.Q., Yang, K.Y., Rice, T.M., Zhang, F.C.: Europhys. Lett. **82**, 17004 (2008)
44. Kane, C.L., Lee, P.A., Read, N.: Phys. Rev. B **39**, 6880 (1989)
45. Martinez, G., Horsch, P.: Phys. Rev. B **44**, 317 (1991)
46. Kampf, A.P.: Phys. Rep. **249**, 222 (1994)
47. Schmailian, J., Pines, D., Stojkovic, B.: Phys. Rev. B **60**, 667 (1999)
48. Kuchinskii, E.Z., Sadovskii, M.V.: J. Exp. Theor. Phys. **88**, 968 (1999)
49. Ovchinnikov, S.G., Korshunov, M.M., Shneyder, E.I.: J. Exp. Theor. Phys. **109**, 775 (2009)
50. Ovchinnikov, S.G., Shneyder, E.I., Korshunov, M.M.: J. Phys. Condens. Matter **23**, 045701 (2011)
51. Stanescu, T.D., Kotliar, G.: Phys. Rev. B **74**, 125110 (2006)
52. Onufrieva, F., Pfenty, P., Kiselev, M.: Phys. Rev. Lett. **82**, 2370 (1999)
53. Senechal, D., Tremblay, A.-M.S.: Phys. Rev. Lett. **92**, 126401 (2004)
54. Senechal, D., Lavertu, P.T., Marois, M.-A., Tremblay, A.-M.S.: Phys. Rev. Lett. **94**, 156404 (2005)
55. Barabanov, A.F., Kovalev, A.A., Urazaev, O.V., et al.: J. Exp. Theor. Phys. **92**, 677 (2001)
56. Plakida, N.M., Oudovenko, V.S.: J. Exp. Theor. Phys. **104**, 230 (2007)
57. Sadchev, S., Chubukov, A.V., Sokol, A.: Phys. Rev. B **51**, 14874 (1995)
58. Chubukov, A.V., Morr, D.K.: Phys. Rep. **288**, 355 (1997)
59. Hosoi, L., Laad, M.S., Fulde, P.: Phys. Rev. B **78**, 165107 (2008)